TECHNICAL NOTE

Calibration of a Three-dimensional Slope Stability Evaluation in Brazilian iron Open Pit Mine

Vidal Félix Navarro Torres · Rodrigo Dockendorff · Juan Manuel Girao Sotomayor [ORCID] **· Cristian Castro · Aristotelina Ferreira da Silva**

Abstract It has historically been frequent among geotechnical practitioners, that the stability analysis of the slopes of an open pit is performed using a two dimensional section representing the highest and steepest walls within a certain geological setting. However, the literature shows that to predict rupture events in an open pit, a three-dimensional analysis would better represent the actual conditions, as the spatial distribution of the lithology and the structural features play an important role when defining the stability of the slopes. This paper presents the case study of an open pit located in Brazil, which experienced instabilities between the years 2001 and 2019. An evaluation of the behavior of the open pit was performed by calibrating the strength parameters to represent the best documented rupture events. The three-dimensional model was made using the finite difference method. The results show that there is a good correlation between the results of the model and the reports of past instabilities. Finally, recommendations are presented for the inter-ramp angles for each lithology based on the calibrated stability analysis performed. This work seeks to contribute to the knowledge in evaluation techniques for the three-dimensional behavior of open pits.

Keywords Open-pit · Slope stability · Calibration · Three-dimensional · Case study

1 Introduction

Commonly, to guarantee an economically profitable while safe mining operation, the stability of the open-pit slopes has been assessed using two-dimensional (2D) analysis. The literature shows that are usually 2D Factor of Safety (FoS) are more conservative than a three-dimensional (3D) analysis (Li et al. 2009; Michalowski 2010; Dana et al. 2018). Several papers presented that 2D analysis in limit equilibrium does not consider the strength generated on the axis parallel to the length of the slope, an effect that does exist in 3D analysis (Lefebvre et al. 1973; Baligh and Azzouz 1975; Leshchinsky and Baker 1986; Saeed et al. 2015; Chakraborty and Goswami 2021; Zebarjadi et al. 2018; McQuillan et al. 2021).Regarding stability analysis performed on open pit slopes, Lam and Fredlund (1993) used a generalized 3D models based on the column method and concluded that the model provides a more realistic simulation compared to a conventional 2D analysis. Stark and Eid (1998) evaluated several historical cases to show the differences

V. F. N. Torres · J. M. G. Sotomayor (✉)
Instituto Tecnologico Vale Mineracao, Belo Horizonte, MG, Brazil
e-mail: juan.sotomayor@itv.org

R. Dockendorff · C. Castro
Itasca Chile, Santiago, Chile

A. F. da Silva
Vale S.A., Parauapebas, PA, Brazil

between 2 and 3D analysis and demonstrated the importance of using a three-dimensional analysis in back-calculating the mobilized shear strength of the materials involved in a slope failure especially in slopes with complicated topography, shear strength conditions, and pore-water pressures. Akhtar (2011) performed a parametric analysis using Finite Element (FE) method, Finite Difference (FD) method and Limit Equilibrium (LE) method based on the assumption that materials along the vertical sides of the slide mass consist of cohesionless material, the result was that all analyses, 3D FoS values are greater than 2D FoS. Wines (2016) studied the differences between 2 and 3D analysis for open pits and found that the main advantage of 3D analysis is the representativeness of the location and orientation of geological structures in relation to a slope and the distribution of different rock mass domains along the strike of a slope, in that sense, the inability of a 2D analysis to represent the true 3D nature of the problem will lead to unrealistic results. Azizi et al. (2018) evaluated the 2D and 3D

stability of an open pit limestone mine, finding that the 2D analysis is very conservative with a significant difference, they also indicated that one of the defects of the 2D analysis is to assume that the width of slope is infinitely wide, which is real in small sections of a slope, but it does not represent all the behavior of a mine wall.

In summary, the application of three-dimensional numerical analysis for open-pits is more appropriate because it can take into account several key factors, such as: topography, hydrogeological conditions, in situ stress, among others, with significant differences compared with two-dimensional analyses (Griffiths and Marquez 2007; Shen and Karakus 2013; Wines 2016; McQuillan and Bar 2023) this is very important for mining activities because responsible mining seeks to ensure maximum recovery of the ore without affecting safety, which can have a significant positive economic effect to the mine (Hoek and Bray 1981; Ali and Morteza 2014; Zevgolis et al. 2018; Utili et al. 2022).

Fig. 1 Iron open pit and instabilities location
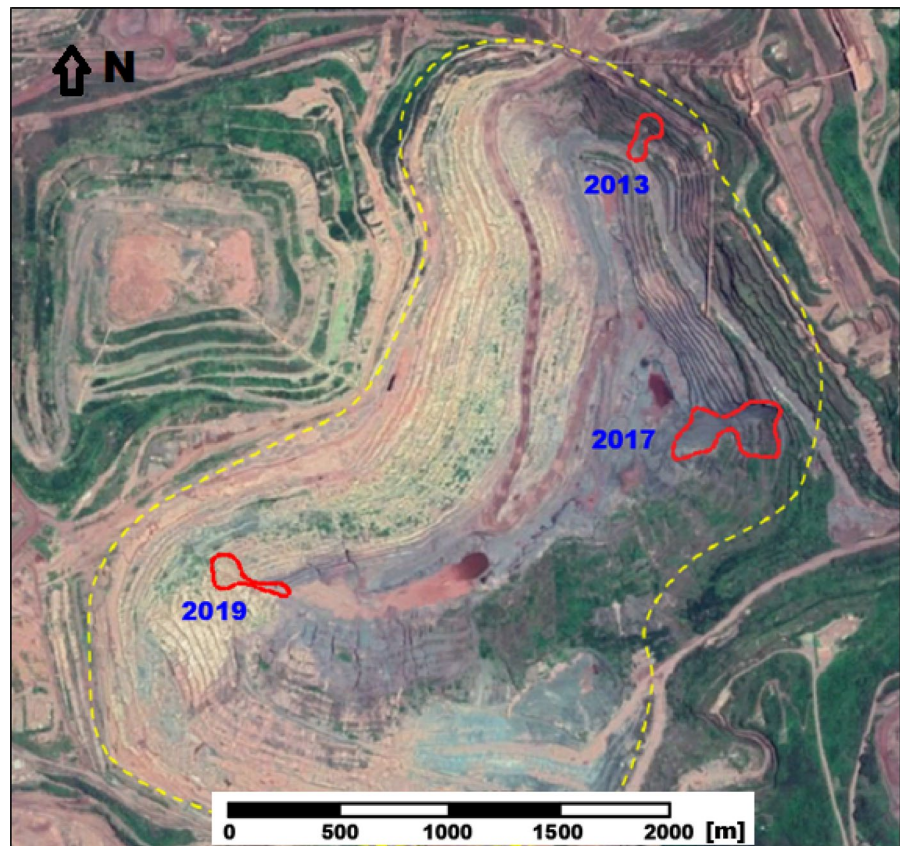
This case study aims to understand the failure mechanisms acting on open-pit slopes in an iron mine located in Brazil (Fig. 1), using a calibrated three-dimensional finite difference method (FDM) software model (Itasca 2011). The open pit slopes vary according to the geotechnical sectorization, but in general the height of the bench is 15 m and the width of the berm is 12 m, the angle range of slopes in friable rocks is 40–70° and in compact 70–85°.

2 Case Description

The study area has experienced fourteen documented instabilities throughout its existence, these events have been distributed in almost all slopes of the mine. The main features of the events were a response to mining advance, the appearance of cracks after the interruption of operations, occurrence of local ruptures due to geological conditions. The events took place in different periods and had different scales as shown in Table 1. Consequently, it is necessary to calibrate the rupture events that occurred to improve the confidence in predicting the future behavior under design geometries.

The main geological structures present are deformations-bands, shear zones and families of joints and faults. The deformation-bands were verified basically in the iron formation and have variable orientations, usually with signs of shear. The surface of the

deformations-bands is sinuous and anastomosed, probably related to shear. The shear planes are generally parallel to the deformation-band of the iron formations and also show high scatter. A shear zone (ZC) occurs in the contact between Ferriferous and Mafic formations, this zone exhibits a high mechanical weathering and low strength parameters. The joints show relatively small persistence and they are found open, filled with talc or carbonate, or closed. Transcurrent faults occur in the mine, orthogonal to sub-orthogonal to shear (in mafic rocks). The main direction of the faults is NW–SE.

In the eastern sector, the shear zone shows NNW-SSE direction and WSW dips (250/38). The joint planes allow the distinction of two main families, one with NNW-SSE direction and the other with ENE-SW, always maintaining medium and high dip angles (maximum 061/64 and 335/86). The kinematic analysis considered three main discontinuities, the shear and two fracture directions, which resulted in the potential of planar failures for this sector (Fig. 2a). The southwest sector presents as main structure the shear zone, whose direction of the plane tends to East–West with dip to the north. The largest plane found for the shear zone was dip direction and dip of 354 and 55, respectively. Joint attitudes show variations in direction while maintaining high dip angles. The largest plane obtained for the joints was dip direction and dip of 186 and 75, respectively. The result of the kinematic analysis does

Table 1 History of ruptures

ID	Period	Sector	Failure mechanisms	Scale	Description
1	2001	South	No data	No Data	Breaks due to the advance of mining
2	2002	South	Circular	No Data	Reactivation of cracks due to work stoppage
3	2002	South	Circular	No Data	Embankment movement with settlements at the top
4	2004	East	Circular	45 m	Slide
5	2005	South	Circular	No Data	Cracks in the slope face
6	2006	Central	Circular	75 m	Slide
7	2007	South	Circular	No Data	Slide
8	2008	Central	Circular	75 m	Slide
9	2009	South	Circular	75 m	Rupture associated with geological conditions
10	2010	South	Circular	45 m	Rupture associated with geological conditions
11	2013	East	Circular	105 m	Rupture associated with geological conditions
12	2017	East	Circular	60 m	Rupture associated with geological conditions
13	2019	South	Circular	120 m	Rupture associated with erosive process
14	2019	South	Circular	150 m	Rupture associated with erosive process
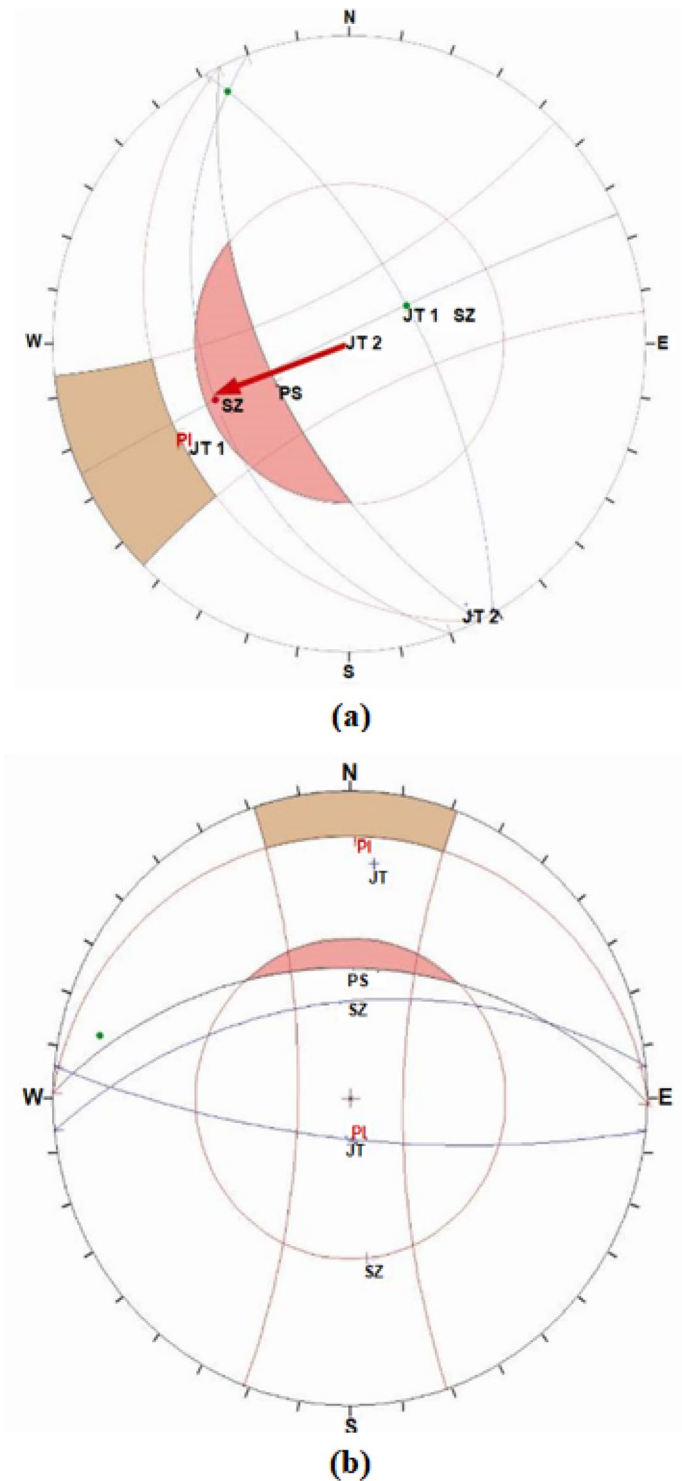
Planes:

ID	Dip Direction/Dip
SZ (Shear Zone)	250°/38°
JT1(Joints)	061°/64°
JT2(Joints)	335°/86°
PS (Pit Slope)	244°/59°
PI (Limit Plane*)	244°/24°

*Slope Dip - friction angle
Friction angle Ø =35°

Results

Planar Sliding = 1
Wedge Sliding = 0
Toppling= 0

(a)

Planes:

ID	Dip Direction/Dip
SZ (Shear Zone)	354°/55°
JT(Joints)	186°/75°
PS (Pit Slope)	001°/44°
PI (Limit Plane*)	001°/09°

*Slope Dip - friction angle
Friction angle Ø=35°

Results

Planar Sliding = 0
Wedge Sliding = 0
Toppling= 0

(b)

Fig. 2 Cinematic analysis **a** east sector **b** southwest sector

not show failure mechanism (planar, wedge and toppling) involving the structures present (Fig. 2b).

A review of the events reported in Table 1 was carried out, finding that the most representative instabilities in the open pit correspond to the years 2013, 2017 and 2019 (Fig. 1), therefore these will be the events used for the calibration process.

The three-dimensional model used the pre-mining topography to represent the initial in situ stress state, then the open pit geometries were evaluated for the above mentioned failure events plus the current condition. The geological block models developed by the mine were used to determine the spatial distribution of the lithology. The failure events used for calibration are detailed below.

The 2013 instability occurred in the East Slope of the main pit, near the access ramp. The failure surface involved 7 benches, each bench is 15 m high, reaching a maximum height of failure of 105 m (Fig. 3). This failure mechanism initially was related to a planar-circular failure with contribution of structural

control of the shear zone, joints did not contribute to overall rupture. After 2013, no significant signs of mass movement or subsidence have been observed in the area.

The 2017 instability occurred in the Upper Part of the East Slope of the main pit, below the main access ramp. The failure surface involved 4 benches, reaching a maximum height of failure of 60 m (Fig. 4). Initially this failure mechanism was related to a combined planar-circular failure, involving as contributing factor the presence of a weak contact (shear zone) between Ferriferous Formation and Metabasic Formation.

The 2019 instability occurred in the South-West Slope of the main pit. The failure surface involved 10 benches, reaching a maximum height of failure of 150 m (Fig. 5). Initially, this failure mechanism was related to a planar-circular failure, and the instability was due to locally insufficient drainage.
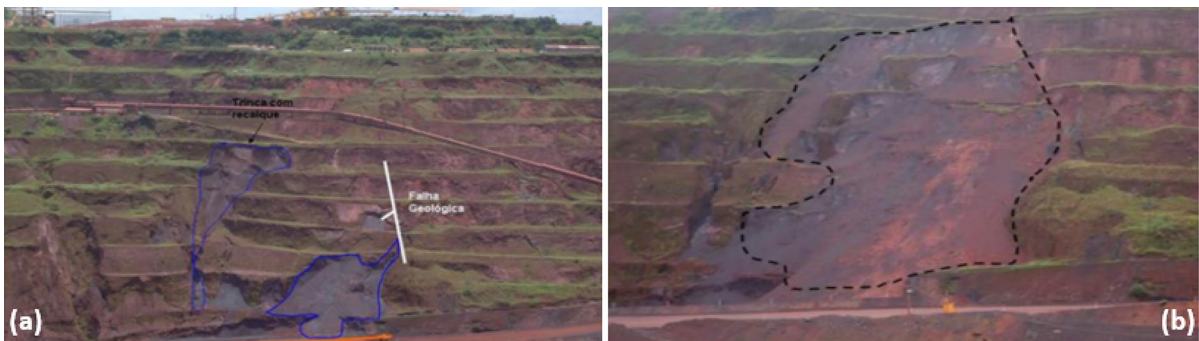

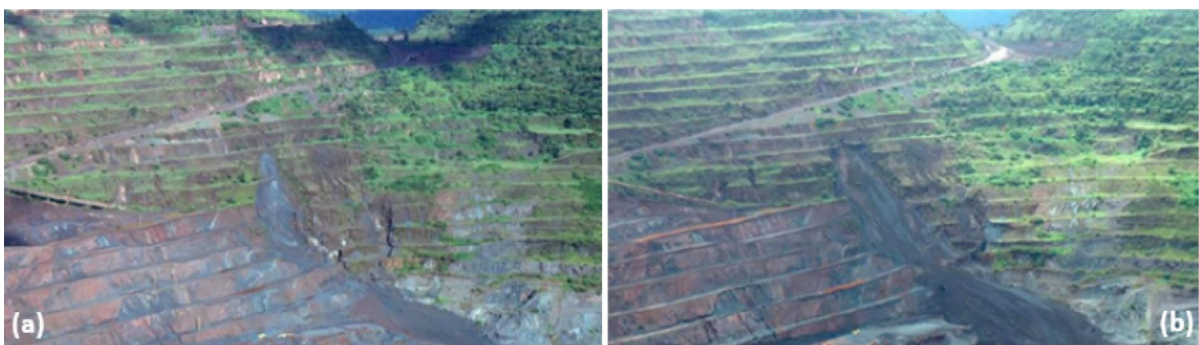**Fig. 3** **a** Pre and **b** post failure condition—east slope (2013)

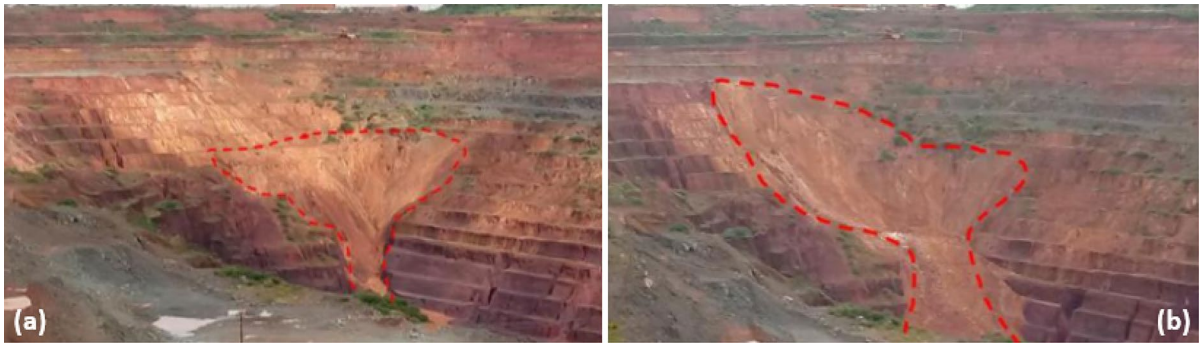**Fig. 4** **a** Pre and **b** post failure condition—east slope (2017)

Fig. 5 **a** Pre and **b** post failure condition—south west slope (2019)

3 Monitoring

The rupture events that occurred in 2013, 2017 and 2019 in the open pit were monitored using instruments installed in these areas, including prism networks, ground radar, piezometers and water level indicators. Daily rainfall data were also used to analyze these events (Fig. 6).

The rainfall that affected the region contributed to the recharge and saturation of the rock mass, allowing the elevation of water levels and the acceleration of movement, where the maximum deformations obtained by terrestrial radars were established around 250 mm (2013), 160 mm (2017) and 3500 mm (2019), as can be seen in Fig. 6b, d, f, respectively. In 2013, due to operational and access conditions, it was not possible to carry out piezometric readings, so that it could follow up the variations during the rains. In 2017, the rainfall accumulated in the month of February reached 469 mm, with the most relevant variations being observed in the vibrating string piezometer (PZCV_02) installed very close to the rupture area, where the piezometric elevation left a level of 641 m and reached the value of 646 m, with the pore pressure recorded around 441 kPa, at 08:27 on 03/12/2017, approximately 30 min before the event (Fig. 7a). In 2019, it is also noted that recharges were significant in the rise of the water level (Fig. 7b).

The precision and periodicity (24/7) of radar monitoring (SSRXT–GroundProbe) enabled more robust and rapid analyses of the displacements occurring in the study areas. The further verification of the beginnings of the accelerations and their progression to rupture was thus possible. This type of monitoring was more effective than other types mainly due to the

speed with which the events occurred, and the results helped with risk management and the decision to block the areas. Table 2 shows some characteristics of failure events.

Monitoring by prisms was concentrated in the area of the ruptures that occurred in 2013 and 2017; however, as it was a conventional survey with periodic readings every two weeks, the analyses were slower and showed indications of progression.

2013—Two prisms showed relevant movements in the 3 axes, ranging from 25 to 90 mm on the X and Y axes and reaching 50 mm on the Z axis.

2017—The prism that best represented the event showed a displacement of 172 mm in the XY direction and a displacement of 35 mm in the Z direction, with a maximum displacement rate of 2.9 mm/day. This fact was confirmed by the greater opening of the established crack and the settlement of the area.

Monitoring was achieved with piezometers and water level indicators established along the pit, and the readings prior to the events showed that some of the instruments presented small increases in the water level, even considering the amount of rainfall that occurred in the period, because the recharge time in the massif is longer.

The rainfall monitoring data show that rainfall events played a role in the events that occurred, as described in Table 3.
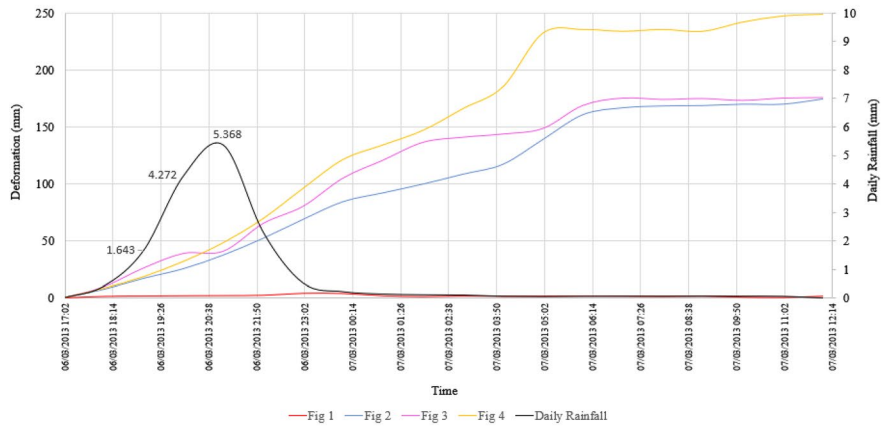
4 Rock Mass Properties

A database of laboratory tests in different lithologies was available at the site to determine the strength parameters. The lithologies with the greatest

Fig. 6 Radar monitoring points and records
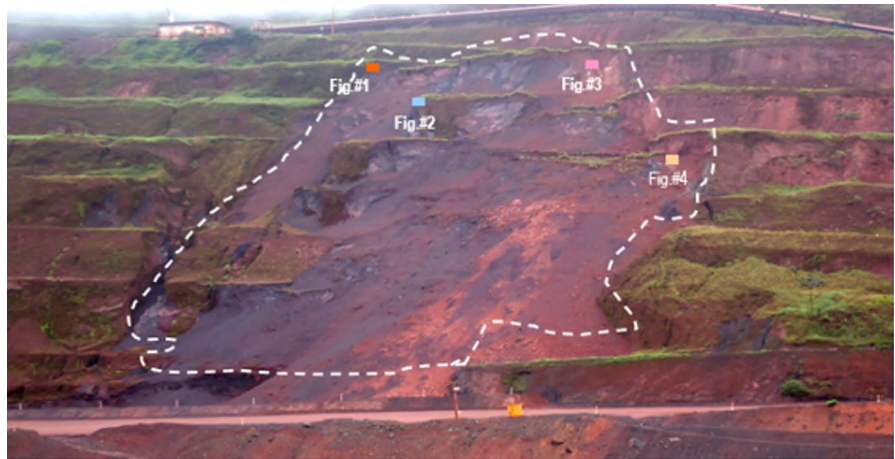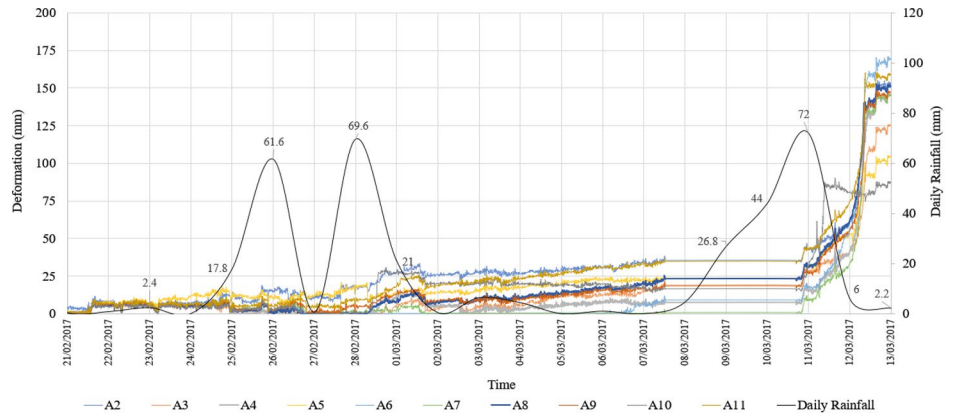

(a) radar localization 2013

(b) radar and rainfall records 2013
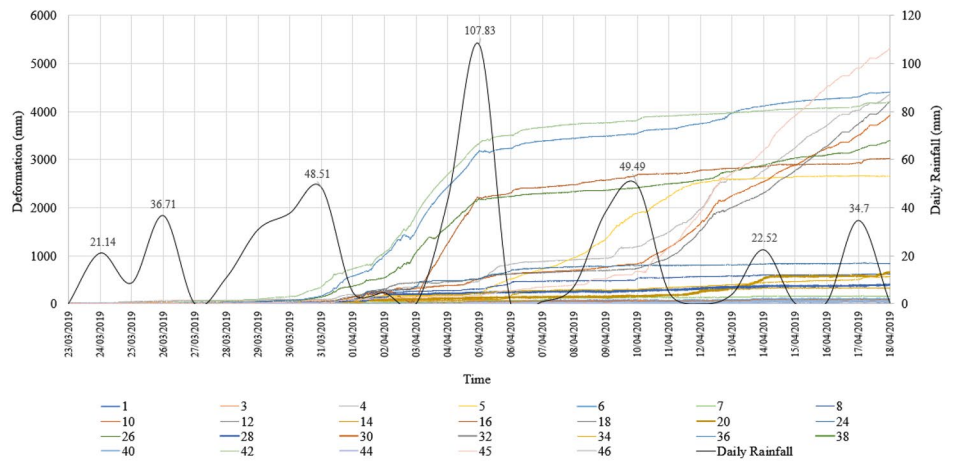

(c) radar localization 2017

Fig. 6 (continued)

(d) radar and rainfall records 2017

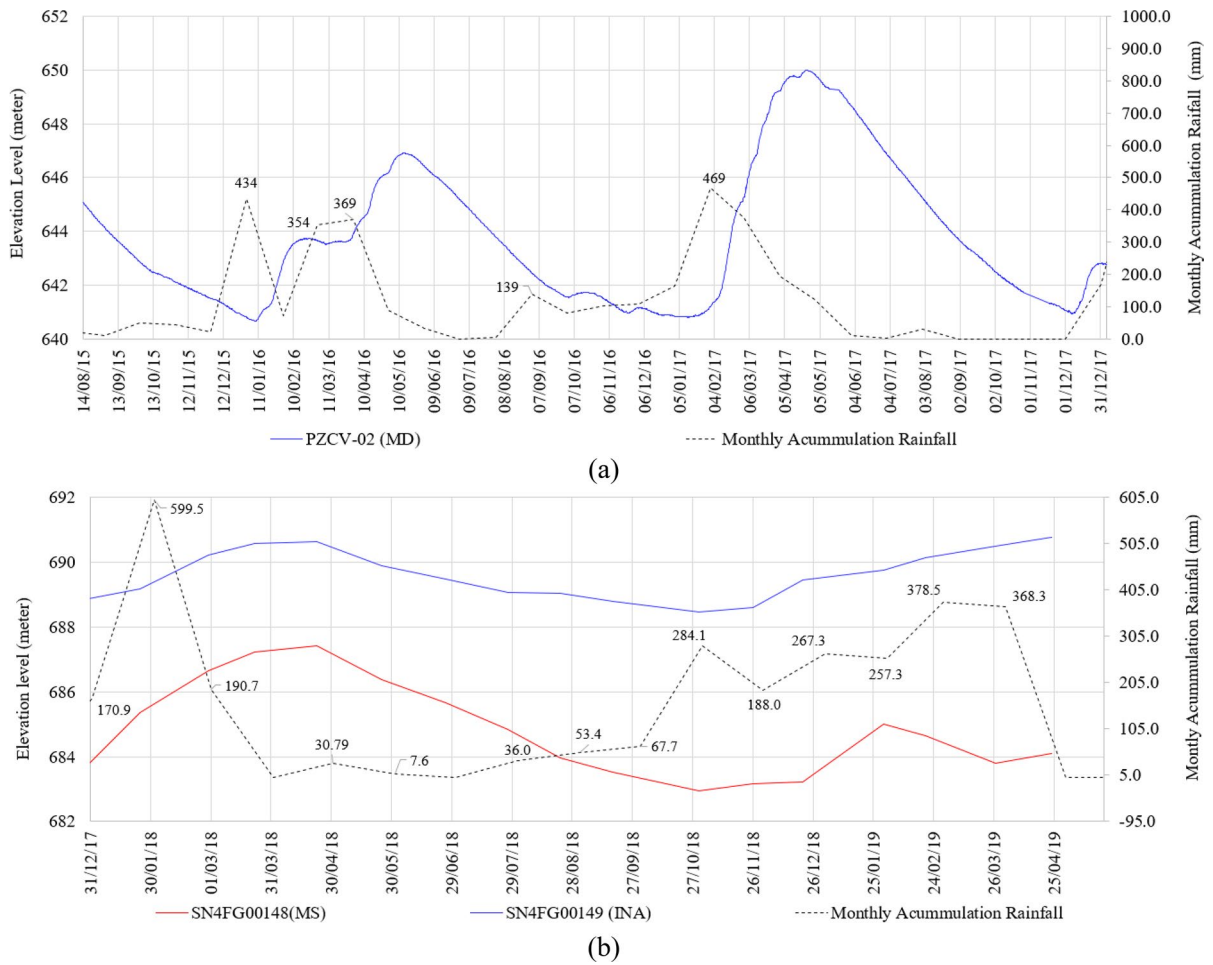(e) radar localization 2019

(f) radar and rainfall records 2019

(a)

(b)

Fig. 7 Piezometers **a** 2017 failure **b** 2019 failure

Table 2 Ruptures events

Event	Day	Peak displacement (mm)	Observation
2013	03/07/2013	250	The accelerations began 24 h before the event
2017	03/12/2017	140	The accelerations began 24 h before the event
2019	04/01/2019	640	The accelerations began 2 days before the event

Table 3 Rainfall events

Event	Period	Cumulative rainfall (mm)	Observation
2013	January–March	700.00	Rainfall occurred at least 3 days before the event
2017	January–March	717.90	72.0 mm of rainfall occurred 1 day before the event
2019	January–April	543.51	23.8 mm of rainfall occurred 1 day before the event

participation in the instabilities correspond to the friable hematite (HF) and decomposed mafic (MD) formations. A total of 38 data points for friable hematite (HF) and 102 data points for decomposed mafic (MD) were used to define the range and variability for the statistical distribution used in the three calibration events. The distribution of the parameters with the most influence on instabilities is shown in Table 4.

A summary of the strength parameters of all lithologies is shown in Table 5 including the shear zone (ZC) mentioned above.

5 Calibration and Validation Process

In the FDM software, the numerical velocity contours are used as a proxy to interpret stability conditions. These velocities (Fig. 8) are given without units, because they are mathematical artifacts and only represent the convergence of the numerical solution. It is Itasca´s experience that numerical velocities greater than $2.5e^{-6}$ after a significant number of timesteps are an indication of unstable behavior, although this reference value needs to be validated on a case-by-case basis.

The calibration process identified the HF, MD and ZC rock units as the main units that control the

documented instabilities along with a structural anisotropy that was represented in the analysis using a ubiquitous joint constitutive model. The set of calibrated parameters can be seen in Table 6. The modeling results representing each rupture event calculated using the calibrated parameters are presented below.

5.1 2013 Calibrated Instability

The model shows a reasonable correlation with the documented 2013 instability (Fig. 8). However, the model overpredicts the Northward extension of the documented failure, the extension to the South, in the East–West axis and in Vertical are reasonable. In Section BB' (Fig. 9) we observe a failure surface that encompasses from level 485 to 620 (failure height of 135 m) reaching a failure depth of 33 m. When compared to the reported failure, which reached a maximum height of 105 m, the model is considered to be reasonable.

It is relevant to notice the role of the shear zone (ZC) in controlling the failure extension. Because of its lower strength, it becomes a referential failure surface, controlling the stability of this area. Due to the above, and by observing the 2013 pit in plan view, it can be noticed that two more areas exhibit unstable behavior (Fig. 10). These areas are controlled by ZC,

Table 4 Data distribution parameters

Rock unit	Cohesion (c', kPa)					Friction angle (ϕ', °)				
	Min	Max	Mean	Median	SD	Min	Max	Mean	Median	SD
Decomposed mafic	0.0	219.0	65.2	35.1	62.2	13.7	41.1	29.5	30.0	5.6
Friable hematite	0.0	258.0	109.7	108.0	72.1	33.0	46.0	39.8	39.8	3.7

Table 5 Summary of strength parameters

Rock Unit	ID	γ_{dry} (kN/m³)	γ_{sat} (kN/m³)	c' (kPa)	ϕ' (°)	JRC	JCS (kPa)	GSI	m_i	σ_c (MPa)
Fresh mafic	MS	29.0	29.0	3200	50	–	–	70	7	151
Semi decomposed mafic	MSD	30.0	30.0	240	32	–	–	60	3	14
Decomposed mafic	MD	18.5	20.0	*	*	–	–	50	2	0.8
Friable hematite	HF	37.0	38.0	*	*	–	–	–	–	–
Compacted hematite	HC	37.0	37.0	250	45	–	–	–	–	–
Jaspelite	JP	37.0	37.0	3750	48	–	–	70	7	167
Canga	CQ	30.0	30.0	65	43	–	–	–	–	–
Shear zone	ZC	19.0	20.0	9	18	8	240	–	–	–

* See Table 4
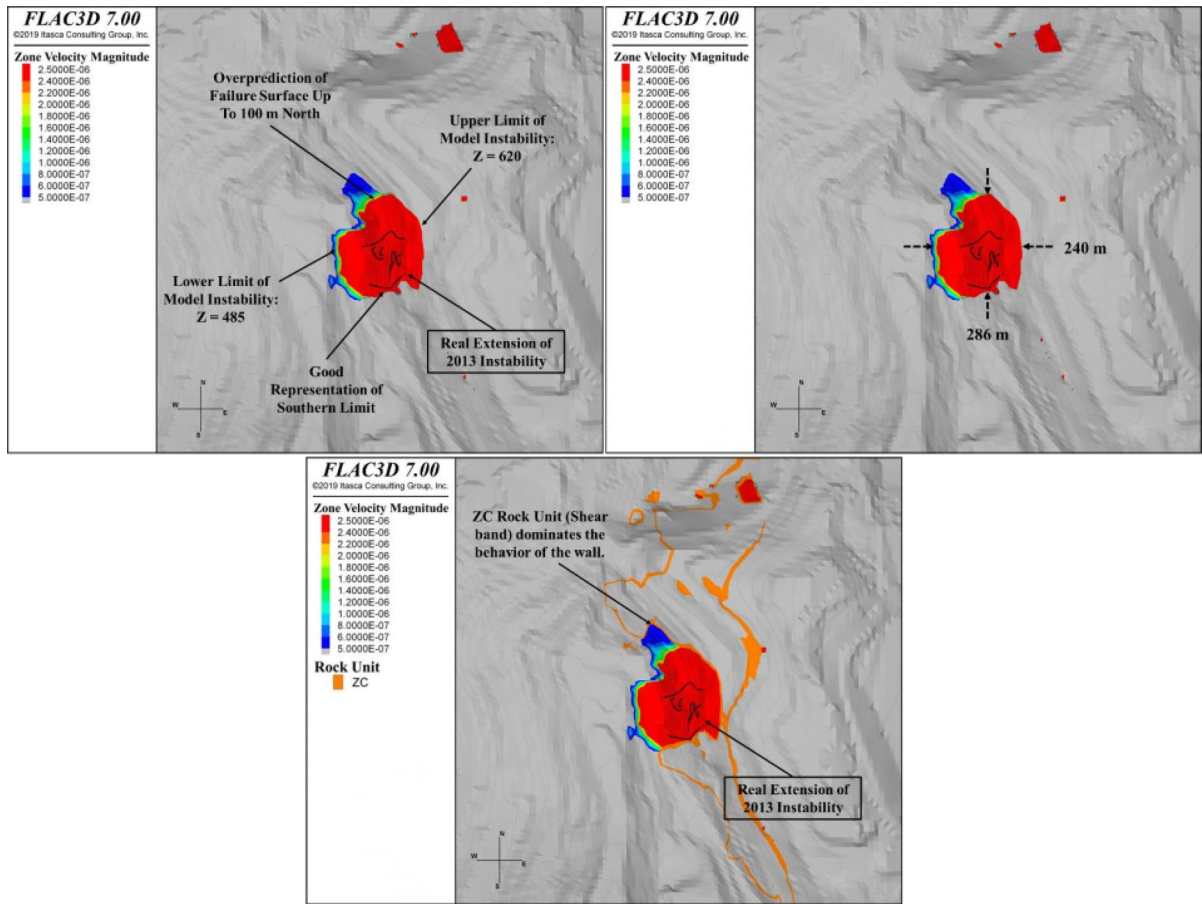
Fig. 8 Results of calibration of 2013 instability

Table 6 Summary of final calibrated properties

Rock unit	ID	γ_{dry} (kN/m³)	γ_{sat} (kN/m³)	c' (kPa)	ϕ' (°)	E_{RM}	ν
Fresh mafic	MS	29.0	29.0	3200	50	29,658	0.22
Semi decomposed mafic	MSD	30.0	30.0	185	26	6405	0.25
Decomposed mafic	MD	18.5	20.0	72	21	426	0.30
Friable hematite	HF	37.0	38.0	95	31	1050	0.28
Compacted hematite	HC	37.0	37.0	250	45	29,658	0.22
Jaspelite	JP	37.0	37.0	3750	48	29,658	0.22
Canga	CQ	30.0	30.0	65	43	200	0.35
Shear zone	ZC	19.0	20.0	7	14	200	0.35
Ubiquitous joints (HF/MD)		N/A	N/A	13	18	N/A	N/A
Ubiquitous joints (Rest.)		N/A	N/A	18	25	N/A	N/A
Faults		N/A	N/A	0	20	N/A	N/A
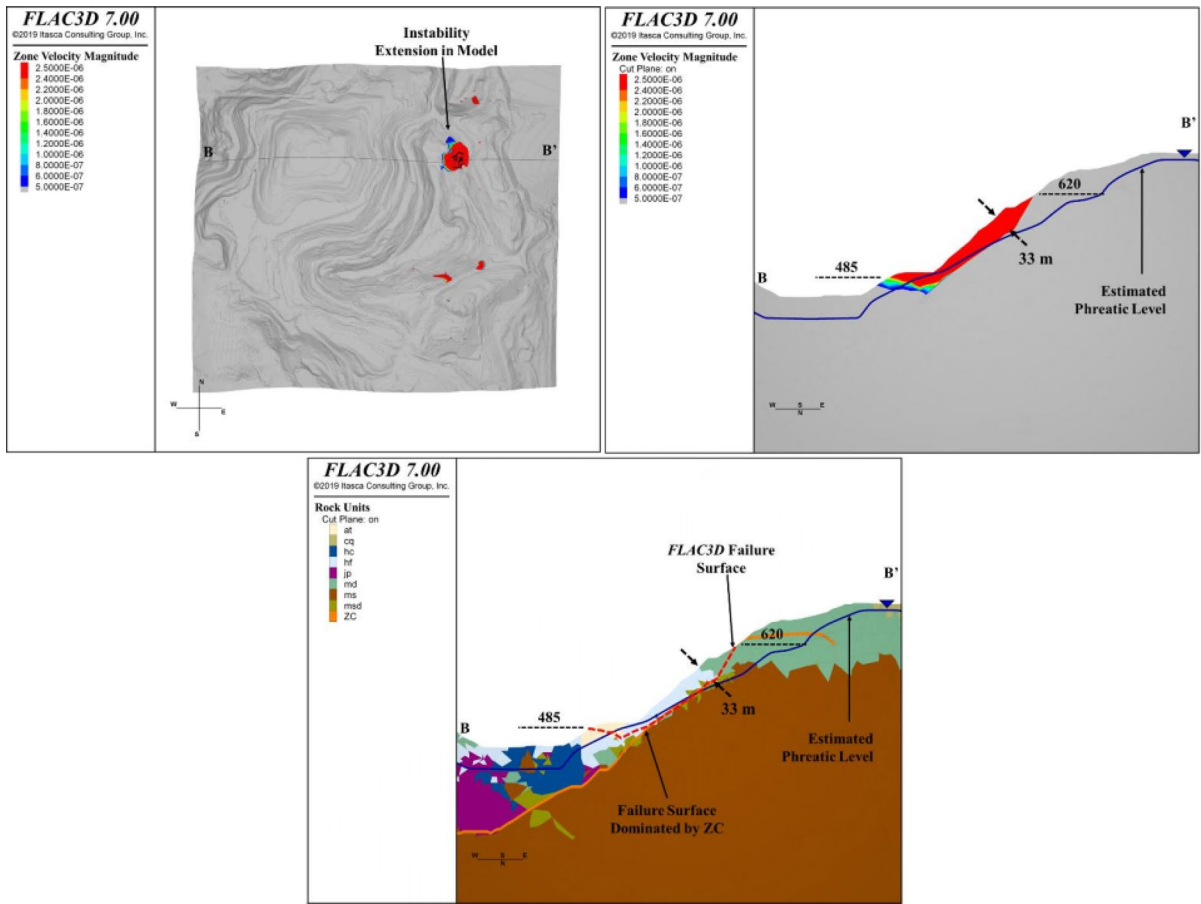
Fig. 9 Results in section B-B'—calibration of 2013 instability
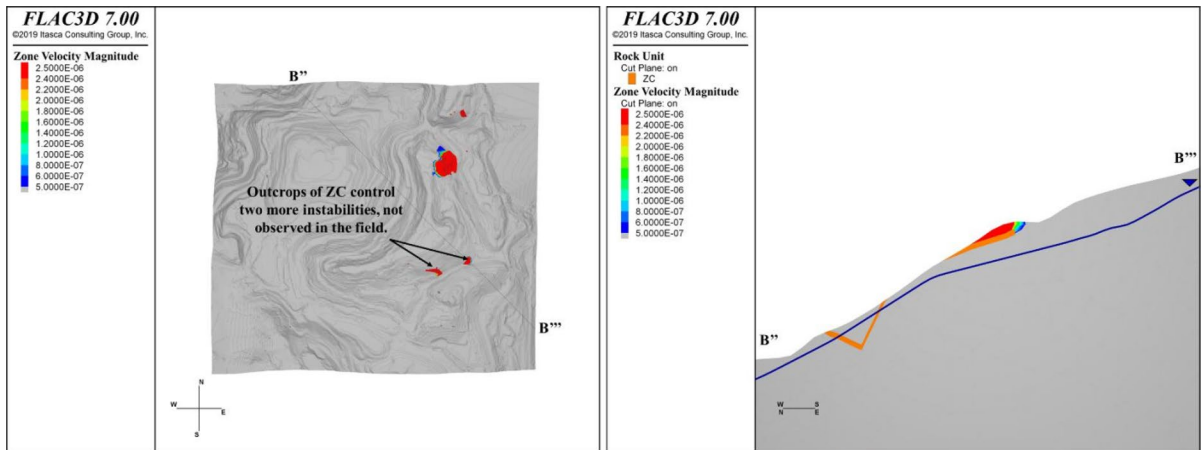
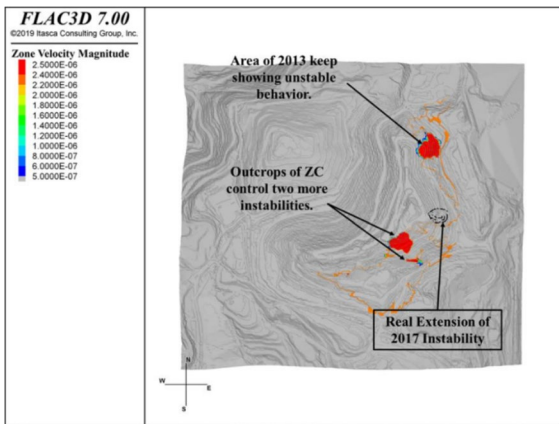**Fig. 10** Effect of ZC—calibration of 2013 instability

Fig. 11 Results of calibration of 2017 instability

sills, because of lack of information. Therefore, the calibration process in this area ended with unsuccessful results.

It is relevant to notice in Fig. 11 that the area of reported instabilities of 2013 remains unstable in 2017. This is due to the fact that the slope does not exhibit a significant change in the overall geometry. Therefore, the slope maintains an unstable condition which does not agree with field observations.

5.3 2019 Calibrated Instability

For the calibration of 2019, the phreatic level was arbitrarily raised up to 20 m below the surface of the pit. This was done in order to reproduce the saturation conditions reported in the documented instability. This approach is aimed at representing the reported lack of proper dewatering in the area where the instability occurred, but unfortunately also over-estimates the influence of water elsewhere outside the failed area. As shown in Fig. 12, the model shows a fair correlation with the documented 2019 instability. When comparing the model prediction against to the documented failure contour, the model reproduces fairly well the extent of the failure in the North and West slopes. The model overpredicts the extension of the failure surface to South, mainly due to the over estimation of saturation and also due to the presence of ZC to the South East.
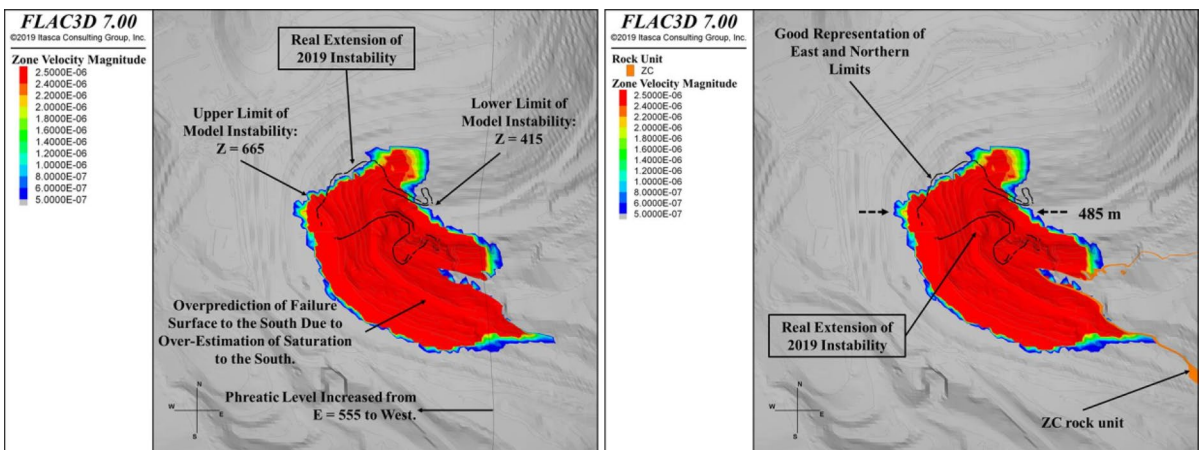
all of them showing the same geometry: Planar failure where the ZC is the failure surface.

5.2 2017 Calibrated Instability

The instability of 2017 could not be reproduced (Fig. 11). After several attempts, it was concluded that more factors need to be added to the model in order to represent the observed behavior. The slope seems to exhibit the occurrence of sills that seem to control the occurrence of the instability. In the Ferrous Rocks, metabasic sills (more rigid rocks within more plastic rocks) occur in concordance with foliation, with widths that range from 0.5 m up to 3 m. The model could not interpret the occurrence of these

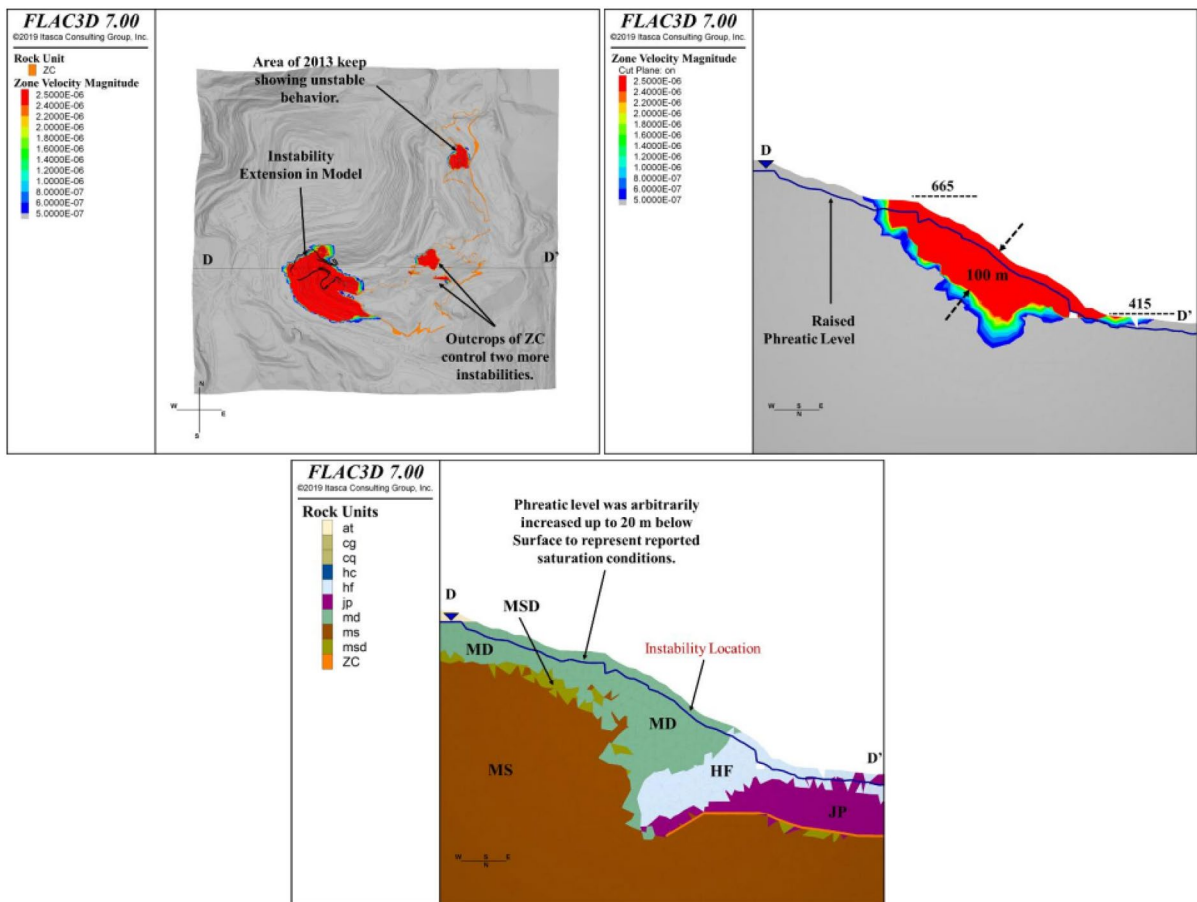**Fig. 12** Results of calibration of 2019 instability

Fig. 13 Results in section D-D'—calibration of 2019 instability

In Fig. 13 the section DD' exhibits a failure surface that involves from level 415 to 665 (failure height of 250 m), reaching a failure depth of 100 m. When compared to the reported failure, which reached a maximum height of 150 m, the model is considered to provide a reasonable yet conservative result considering the assumption of rising the phreatic level.

5.4 Validation of Calibrated Parameters (2019 current pit)

With the set of calibrated parameters, the 2019 current pit was evaluated as a means to validate the properties derived. To do so, velocity contours are shown in Fig. 14 and Fig. 15.

The calibrated set of parameters remain conservative. In Fig. 14 it is observed that the area of 2013

instability remains unstable. This again is due to the small change in the geometry in this sector. While the 2013 area shows unstable behavior due to geometrical reasons, there are a few more areas of unstable behavior. In the South of the open pit, three areas exhibit unstable behavior, but again these areas are related to planar-circular failures formed by the influence of the shear zone. Another area of unstable behavior locates at the toe of the West Slope (Fig. 15). The numerical model, in this region, exhibits toppling at the toe. This toppling mechanism spreads upward the deformation in the lower part of the West Slope (Interramp Angle or IRA ~ 37°). This could suggest conservative calibrated parameters, or changes in the joint orientations in this area which are not documented in the geotechnical model.

Nonetheless, due to the reasonable representation of the past instabilities and although conservative, it
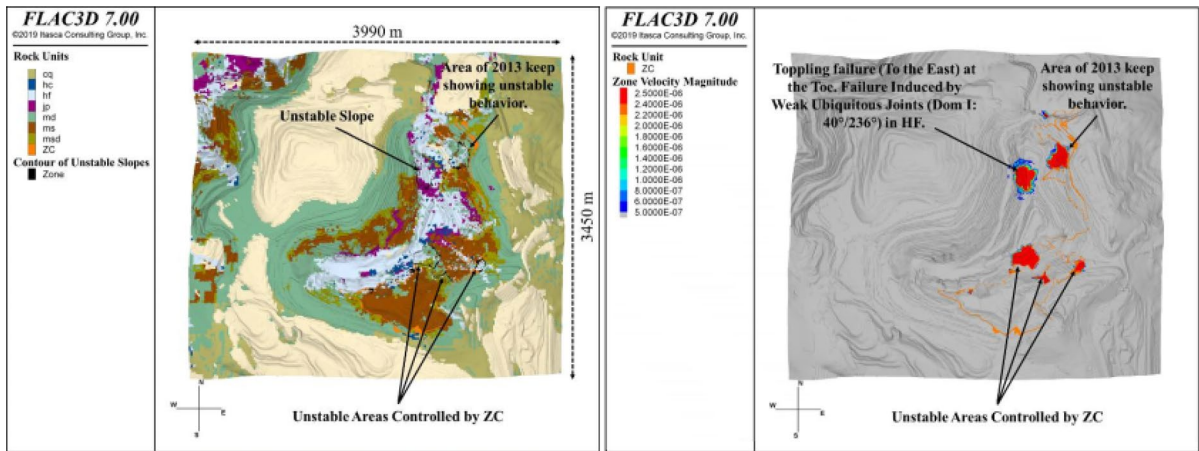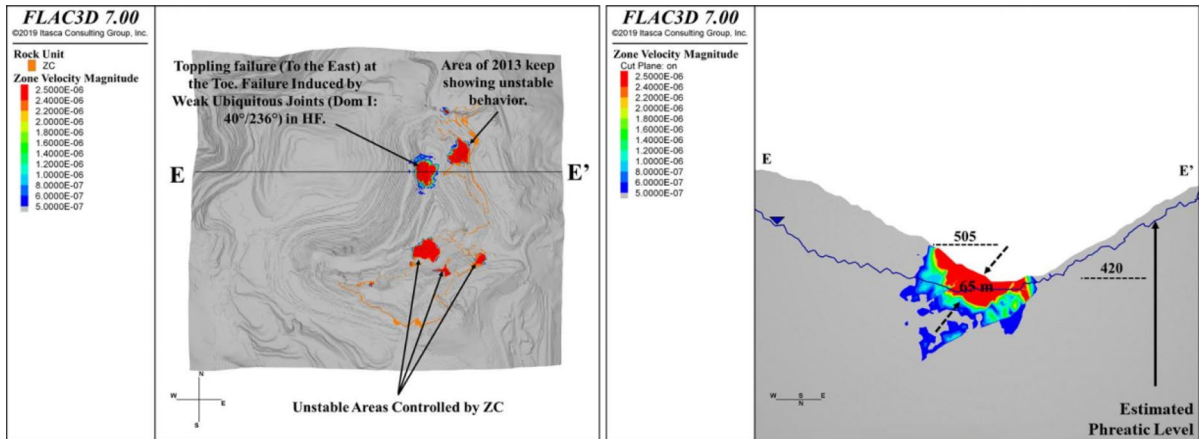
Fig. 14 Velocity contours—2019 current pit

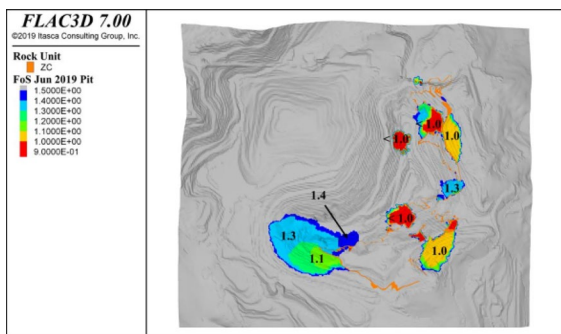**Fig. 15** Velocity contours in section EE'—2019 current pit

Fig. 16 FoS current pit

is deemed that the new set of parameters can be used to evaluate future design geometries of the open pit.

6 Stability Analysis

The analysis was divided into three stages: (a) the first, aimed to assess the stability condition of the current pit (Fig. 16), by characterizing the rock mass with the set of calibrated parameters considering the water table position and calculating Factors of Safety (FoS) using the Shear Strength Reduction (SSR)
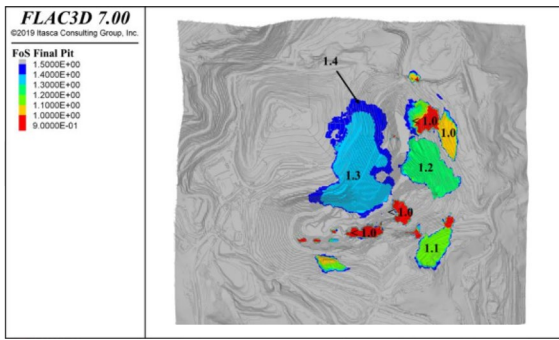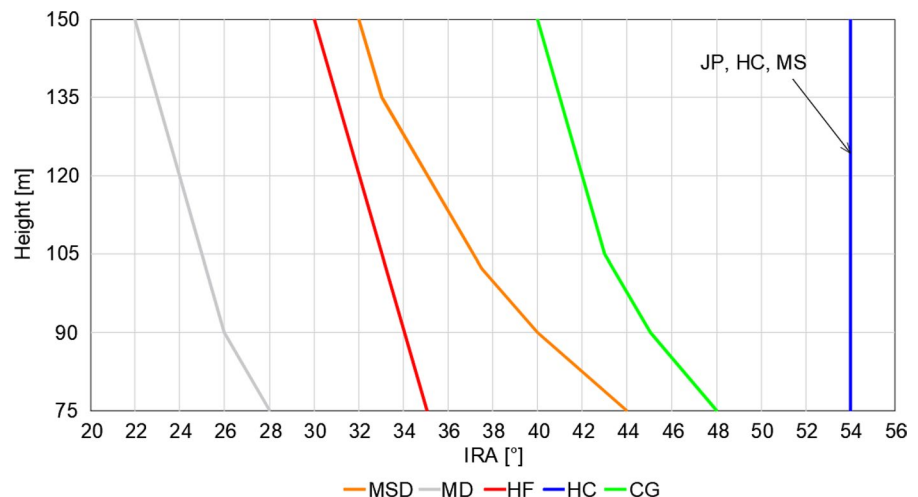
Fig. 17 FoS final pit

technique; (b) the second is intended to advice the mine with IRA recommendations for each rock unit, in terms of the calibrated parameters established; (c) finally, the stability of a future open pit geometry is evaluated (Fig. 17).

When comparing FoS contours for current and future pit, two behaviors can be noticed:

All the sectors with FoS ≤ 1.1 remain "unstable", this is due to:

- Occurrence of unstable behavior of the area of 2013 instability, which remains with essentially no changes in its geometry.
- Geometries of "planar failure" controlled by ZC during this time period.
- Due to mining of the future pit, two large sectors exhibit 1.2 ≤ FoS ≤ 1.3. This occurs in the West Slope and in the East Slope.

- In the west, the slope shows a FoS ≥ 1.3 due to the increase in the IRA. In this sector of the mine, the rock mass is characterized by MD unit, controlling the failure mainly through the rock matrix, because the joint sets dip -59° (Considering IRA-31–40°).
- In the East, the slope shows a FoS ≥ 1.2 due to the role of ZC in forming a geometry of "planar failure" contained by a rock bridge composed mainly by HF unit. Most of the final pit shows an acceptable stability condition (i.e. FoS ≥ 1.3).

7 Ira Recommendations

The IRA recommendations were developed using a simplified two-dimensional FDM software analysis, considering that the analyses were carried out in dry conditions. The dry condition was evaluated considering that the mine is able to perform adequate drainage in the open pit, for the current conditions this assumption must be considered carefully, because the phreatic levels have proven to be a critical contributor to instabilities in the open pit. The acceptability criteria was: FoS ≥ 1.3.

For the rock units in the mine, they were assessed using only the rock matrix without any faulting or joint sets. This included: MS, MSD, MD, HC, HF, JP and CQ. Due to the importance of joint sets in the HF and MD behavior, according to the results shown previously, it was also assessed the IRAs including the most unfavorable orientations per each that could
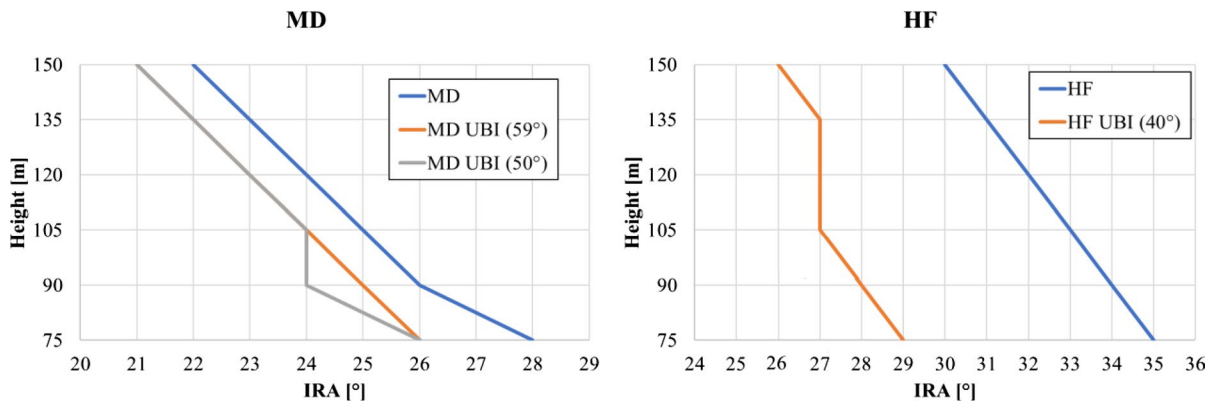
Fig. 18 Design chart (without joint sets) for a FoS of 1.3 and under dry conditions

Fig. 19 Design charts for MD and HF (with ubiquitous Joints), for a FoS of 1.3 and under dry conditions

be found in the model. The joints were modeled with c = 13 kPa and ϕ = 18°. The design charts without and with joints are shown in Figs. 18, 19. The recorded planar-circular failures had no influence on the joints, the IRA recommendation chart seeks to answer what would be the effect of finding in the future the worst condition in joint orientation in the lithologies where the ruptures occurred.

In Fig. 18, considering ubiquitous joints in the lithologies, it is observed that for a slope height of 120 m in HF and MD rocks, the recommended inter-ramp angle is 32° and 24°, respectively. In the most unfavorable case of rocks with ubiquitous joints (Fig. 19), for the same height of 120 m in HF and MD rocks the recommended inter-ramp angle is 27° and 23°, respectively. It is noted that the presence of ubiquitous joints has a great influence on the stability of the HF lithology, so a constant field mapping must be carried out in order to identify the distribution of discontinuities.

8 Conclusions

The work describes the calibration process of a 3D stability model of an open pit located in Brazil. Three documented instabilities located in different areas of the open pit were used in the calibration process of the strength parameters for each lithology.

The calibration process identified the HF, MD and ZC rock units as the main units that control the documented instabilities along with ubiquitous joints.

As stated during the work, a conservative approach was used, all the joints were treated the same in the numerical modeling. Although during the calibration process the joint sets that outcrop in HF and MD were treated differently, there were no documented differences between shear and bedding planes that could induce differences in the behavior of the slopes.

During the calibration, the numerical model confirmed the influence of the shear zone between the ferriferous formation and the mafic formation on the recorded instabilities, therefore it is necessary to map this zone in more detail during the final open pit formation. Also, the calibration verified the influence of the water level on the registered instability; therefore, improving the mine's drainage system is essential to reduce this effect in the future.

Finally, the model is considered acceptable, representing the current conditions of the open pit and as a result of the model, recommendations for inter-ramp angle were made for each lithology for a future open pit geometry, taking into account the maximum material removal in a safe and economically profitable way.

Data Availability Enquiries about data availability should be directed to the authors.

Declarations

References

Akhtar, K. (2011). Three-dimensional slope stability analyses for natural and manmade slopes. University of Illinois at Urbana-Champaign. http://hdl.handle.net/2142/24459

Ali MA, Morteza O (2014) Determination and stability analysis of ultimate open-pit slope under geomechanical uncertainty. Int Min Sci Technol 24(1):105–110

Azizi MA, Marwanza I, Amala SA, Hartanti NA (2018) Three-dimensional slope stability analysis of open pit limestone mine in Rembang District, Central Java. In: IOP conference series: earth and environmental science. IOP Publishing. vol 212(1). p 012035

Baligh M, Azzouz AS (1975) End effects on stability of cohesive slopes. J Geotech Eng Div ASCE 101(GT11):1105–1117

Chakraborty A, Goswami D (2021) Three-dimensional slope stability analysis using stability charts. Int J Geotech Eng 15(5):642–649

Dana H, Kakaie K, Rafiee R, Bafghi A (2018) Effects of geometrical and geomechanical properties on slope stability of open-pit mines using 2D and 3D finite difference methods. J Min Environ 9(4):941–957

Griffiths D, Marquez R (2007) Three-dimensional slope stability analysis by elasto-plastic finite elements. Geotechnique 57(6):537–546

Hoek E, Bray JD (1981) Rock slope engineering: 3rd ed. CRC Press. https://doi.org/10.1201/9781482267099

Itasca F (2011) Fast lagrangian analysis of continua in 3 dimensions V. 5, user's guide. Itasca Consulting Group, Minneapolis, Minnesota, 318–308

Lam L, Fredlund D (1993) A General limit equilibrium model for three dimensional slope stability analysis. Can Geotech J 30:905–919

Lefebvre G, Duncan J, Wilson E (1973) Three dimensional finite element analysis of dams. J Soil Mech Found Div ASCE 99(7):495–507

Leshchinsky DOV, Baker R (1986) Three-dimensional slope stability: end effects. Soils Found 26(4):98–110

Li AJ, Merifield RS, Lyamin AV (2009) Limit analysis solutions for three-dimensional undrained slopes. Comput Geotech 36:1330–1351

McQuillan A, Bar N, Yacoub T (2021) On the comparison of 2D and 3D stability analyses of an anisotropic slope. In: Hammah RE, Yacoub TE, McQuillan A, Curran J (eds) The evolution of geotech—25 years of innovation. CRC Press, London, pp 295–306. https://doi.org/10.1201/9781003188339-38

Mcquillan A, Bar N (2023) The necessity of 3D analysis for open-pit rock slope stability studies: theory and practice. J South Afr Inst Min Metall 123(2):63–70

Michalowski RL (2010) Limit analysis and stability charts for 3D slope failures. J Geotech Geoenviron Eng 136(4):583–593

Saeed MS, Maarefvand P, Yaaghubi E (2015) Two and three-dimensional slope stability analyses of final wall for Miduk mine. Int J Geo-Eng 6(1):9

Shen J, Karakus M (2013) Threedimensional numerical analysis for rock slope stability using shear strength reduction method. Can Geotech J 51(2):164–172

Stark TD, Eid HT (1998) Performance of three-dimensional slope stability methods in practice. J Geotech Geoenviron Eng 124(11):1049–1060

Utili S, Agosti A, Morales N, Valderrama C, Pell R, Albornoz G (2022) Optimal pitwall shapes to increase financial return and decrease carbon footprint of open pit mines. Min Metall Explor 39:335–355. https://doi.org/10.1007/s42461-022-00546-8

Wines D (2016) A comparison of slope stability analyses in two and three dimensions. J South Afr Inst Min Metall 116(5):399–406

Zebarjadi D, Khaloo R, Rafiee R, Yarahmadi A (2018) Effects of geometrical and geomechanical properties on slope stability of open-pit mines using 2D and 3D finite difference methods. J Min Environ 9(4):941–957

Zevgolis IE, Deliveris AV, Koukouzas NC (2018) Probabilistic design optimization and simplified geotechnical risk analysis for large open pit excavations. Comput Geotech 103:153–164